Correction published 2 June 2004

Iron charge state distributions as an indicator of hot ICMEs: Possible sources and temporal and spatial variations during solar maximum

S. T. Lepri and T. H. Zurbuchen

Space Physics Research Laboratory, University of Michigan, Ann Arbor, Michigan, USA

[1] It has been shown that Fe charge states greater than and equal to 16 are often observed in the presence of interplanetary coronal mass ejections (ICMEs) at 1 AU. These elevated charge states, representative of hot source regions on the Sun, provide an identifier of ICMEs independent of expansion processes and heliocentric distance. Using this new identifier, we present a comparative study of Fe charge state distributions as a function of latitude and time. We compare Fe charge state data from the ACE spacecraft in the ecliptic plane with that from the Ulysses spacecraft along its orbit from low to high latitudes. We discuss the frequencies of high Fe charge state distributions through a range of latitudes on the approach toward solar maximum. Close to solar maximum, we find almost an order of magnitude fewer hot ICMEs at higher latitudes than in the ecliptic. We offer an explanation for the existence of high Fe charge states in hot ICMEs as a result of magnetic connectivity to flaring regions. *INDEX TERMS:* 7513 Solar Physics, Astrophysics, and Astronomy: Coronal mass ejections; 7599 Solar Physics, Astrophysics, and Astronomy: General or miscellaneous; 2162 Interplanetary Physics: Solar cycle variations (7536); 7509 Solar Physics, Astrophysics, and Astronomy: Corona; 7519 Solar Physics, Astrophysics, and Astronomy: Flares; *KEYWORDS:* coronal mass ejections, solar wind ionic composition, flares, Fe (iron), minor ions, interplanetary CMEs

Citation: Lepri, S. T., and T. H. Zurbuchen (2004), Iron charge state distributions as an indicator of hot ICMEs: Possible sources and temporal and spatial variations during solar maximum, *J. Geophys. Res.*, *109*, A01112, doi:10.1029/2003JA009954.

1. Introduction

[2] The solar wind flows away from the Sun steadily carrying mass into interplanetary space. Transient, violent explosions of magnetic field accelerate coronal material out from the Sun into the solar wind in the form of interplanetary coronal mass ejections (ICMEs). (Henceforth, we will use the term ICME to refer to the interplanetary manifestation of coronal mass ejections (CMEs) and the term CME to mean the coronal mass ejection observed launching from the Sun's surface in coronagraph images.) The material ejected into ICMEs directly affects the Earth and its surroundings, making the in situ exploration of ICME-related material an important aspect of space physics.

[3] Since the 1970s, ICMEs have been observed from ground-based and space-based instruments [*Hundhausen*, 1993, and references therein]. These data have allowed access to the temporal and spatial variations of ICMEs. In general, the frequency of ICMEs follows the solar cycle with significantly more events occurring at and around solar maximum [*Webb and Howard*, 1994]. However, observations of CMEs indicate that the ejecta are not uniformly distributed in the heliosphere. Coronagraph observations and in situ measurements indicate a deficit of ICMEs at high latitudes, even in years near solar maximum when the coronal magnetic field is much less ordered [*McComas et al.*, 2001; *Burkepile and St. Cyr*, 1993; *Hundhausen*, 1993].

Using data from spacecraft, such as Ulysses, in conjunction with data from spacecraft orbiting in the ecliptic, we continue to study ICMEs as they propagate through the heliosphere.

[4] Many signatures characteristic of ICMEs have been reported in previous statistical studies [e.g., *Gosling*, 1990, and references therein; *Neugebauer et al.*, 1997]. Some of those signatures include the presence of bidirectional electrons (BDEs), specific velocity and density profiles [*Gosling and Riley*, 1996], certain magnetic field topologies [*Burlaga*, 1991; *Gosling*, 1990], and various compositional signatures such as He enhancements and anomalous charge states [*Borrini et al.*, 1982]. Significant variations of the individual ICME identifiers have been observed at 1 AU. These variations may be due to spatial structures of the ICME plasma in the structure of the ICME source region [*Antiochos*, 1998]. ICMEs have also been observed at 1 AU that retain these spatially distinct particle populations [*Haggerty et al.*, 2000; *Skoug et al.*, 2000]. As a result, the signatures may depend upon the observational cut through the ICME and its properties close to the Sun. Unlike most other signatures, compositional signatures are independent of radial distance from the Sun as well as plasma interactions. These characteristics make them ideally suited for the identification of ICMEs over a large range of heliospheric distances.

[5] Several case studies and surveys have identified anomalously high ionization states in ICMEs [*Fenimore*, 1980; *Henke et al.*, 1998; *Gloeckler et al.*, 1999]. In our earlier study [*Lepri et al.*, 2001], it was shown that at least

92% of enhanced ratios of $Fe^{\geq 16+}/Fe_{Tot}$ that persist for 20 hours or longer relate to ICMEs in observations from the Advanced Composition Explorer (ACE) spacecraft (using data from 1998 to the middle of 2000). However, the reverse correlation of ICMEs with high Fe charge states (Q_{Fe}) is not as good (averaged over 1998–2002, at least 63% of ICMEs exhibit high Fe charge states). These correlations imply that the high Fe charge states are not a necessary condition but an excellent sufficient signature of ICMEs. The near 100% correlation of high Q_{Fe} with ICMEs makes them one of the best identifiers of ICMEs.

[6] Since we observe charge states characteristic of high source region temperatures capable of producing high Q_{Fe}, hereafter we will refer to these ICMEs as "hot ICMEs" (when we refer to temperatures, we mean freeze-in temperatures, which are approximated by the electron temperature for collisional equilibrium). In steady state solar wind conditions, Fe charge states freeze in within $3–4$ $R_\odot$ from the Sun and remain unchanged as the particles travel through interplanetary space [*Bame et al.*, 1974; *Bürgi and Geiss*, 1986]. In this way, charge state information is unique: it is independent of radial distance from the Sun (beyond the freeze-in radius) and for the most part unaffected by plasma interactions, therefore making charge states one of the best signatures for identifying ICMEs over a range of heliocentric radii. For these reasons, charge state information can be used to probe the physical properties of the inner corona [*Owocki et al.*, 1983]. Different charge distributions characterize different source regions in the corona. It is the aim of this paper to extend the methods and results of *Lepri et al.* [2001] in order to compare ACE data with Ulysses data from its 1998–2002 journey over the Sun's magnetic poles. We will use $\langle Q \rangle_{Fe}$ instead of $Fe^{\geq 16+}/Fe_{Tot}$ as an identifier over these periods and ranges of heliocentric distance due to the better statistics attained with charge state information. Here, $\langle Q \rangle_{Fe}$ is the average charge state of Fe defined as $\langle Q \rangle_{Fe} = \Sigma_i Q_i n_i$, where density is normalized such that $\Sigma_i n_i = 1$. The ratio $Fe^{\geq 16+}/Fe_{Tot}$ is defined as $\Sigma_{i>15} n_i$. The identifier $\langle Q \rangle_{Fe}$ can then be used with Ulysses data, in which $\langle Q \rangle_{Fe}$ is the most reliable indicator of Fe charge state behavior. These combined data should reveal temporal and spatial variations in the solar corona.

[7] ACE data are analyzed from the hot ICME time periods defined by *Lepri et al.* [2001] and the results are used to determine a threshold average charge state characteristic of hot ICMEs. In our previous study, hot ICME periods were defined as those two hour bins with the relative charge state abundances, $Fe^{\geq 16+}/Fe_{Tot} > 0.1$, that persisted for at least 20 hours (10 consecutive data points). The development of the $\langle Q \rangle_{Fe}$ as an identifier of hot ICME material allows us to translate the methods of *Lepri et al.* [2001] to the data from the Solar Wind Ion Composition Spectrometer (SWICS) on Ulysses. Comparing charge state data from ACE and Ulysses provides insight into physical processes observed in the ecliptic (from both ACE and Ulysses at the start of 1998) and at a range of latitudes extending toward the solar poles (Ulysses through the end of 2002) near solar maximum. We determine the fraction of time both ACE and Ulysses spend in ICME-associated flows over a range of latitudes. We use these data to investigate the isotropy or lack thereof in the heliosphere during solar maximum and consider the physical processes that could lead to anomalous charge state distributions.

2. Observations

[8] The Fe charge state distributions were obtained aboard the ACE and Ulysses spacecraft using their SWICS instruments [*Gloeckler et al.*, 1998, 1992]. ACE, launched in 1997, orbits about the L1 point, $\sim$240 Earth radii upstream from Earth. Ulysses, launched in 1990, embarked on an orbit that would eventually take it on several passes over the poles of the Sun. The SWICS instruments operate similarly on both the ACE and Ulysses spacecraft and are able to determine the density, bulk, and thermal speeds of almost 40 heavy-ion species. This information enables one to calculate the charge state distributions and abundances of 10 elements, including Fe.

[9] The SWICS instrument is a time-of-flight (TOF) mass spectrometer with an energy-resolving solid-state detector (SSD). Ions are mass and speed selected and residual energy measured at the solid-state detector enables particle identification. The determinations of mass M, charge Q, and energy E are virtually free of background contamination due to the triple-coincidence technique employed (detecting a time-of-flight "start," "stop," and SSD energy signal). The data are corrected for event priorities, instrument efficiencies, and duty cycle. In particular, we identify Fe charges states between 4 and 24 in the energy-per-charge (E/Q) range of 0.49–100 keV/e. SWICS on Ulysses cannot provide the density of a particular Fe charge state on a time scale less than 2 hours due to limited statistics at large heliocentric radii. Fe charge state information from SWICS on Ulysses was obtained from the Internet (available at http://helio.estec.esa.nl/Ulysses/Archive/). The data are processed into 3-hour averages using routines described by *von Steiger et al.* [2000]. The Fe charge state data from ACE are calculated in a similar manner (see *Lepri et al.* [2001] for methodology). From count rates, we determine the phase space density for the different ionic charge states of Fe with a time resolution of 12 min. However, to improve statistics, and in order to match the resolution of the Ulysses SWICS data, we average our data over 3-hour intervals. Using the phase space density, n_i (where i numbers the ionic charge states of Fe from 4 to 24), we can calculate the average charge states $\langle Q \rangle_{Fe}$. The charge state data from ACE are accurate to better than 10%; Ulysses charge states are accurate to 25% [*von Steiger et al.*, 2000].

3. Analysis

[10] In order to define a threshold value for $\langle Q \rangle_{Fe}$ above which it would likely be associated with an ICME as determined by *Lepri et al.* [2001], we created a histogram in increments of $0.2 \langle Q \rangle_{Fe}$ for the ACE data from the entire year of 1999. Figure 1a shows the histogram representing the normalized occurrence rate of certain charge states as defined by normal solar wind and hot ICME-related solar wind. Normal solar wind periods are intended to be periods of quiescent solar wind and are taken immediately before or immediately after the ICME, and do not show composition enhancements (such as in the O^{7+}/O^{6+} ratio; $O^{7+}/O^{6+} > 0.7$ provides a complementary identifier for the presence of ICME material [*Reinard et al.*, 2001]). For consistency and

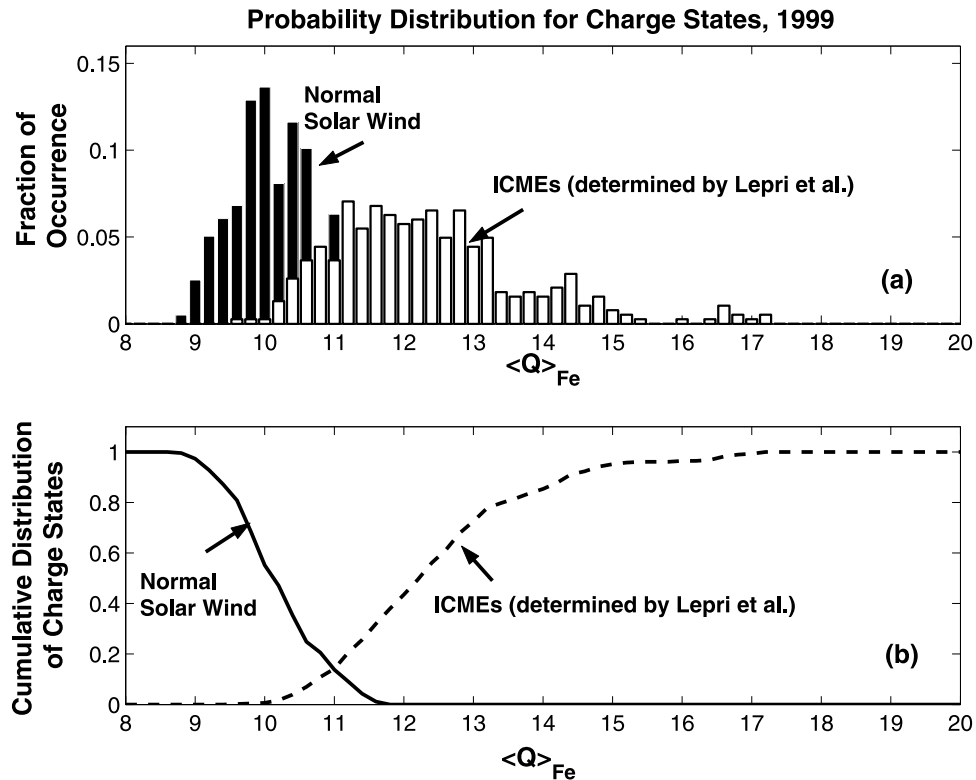**Probability Distribution for Charge States, 1999**

Figure 1. (a) Histogram representing the normalized occurrence rate of certain Fe charge states in normal solar wind and hot ICME [*Lepri et al.*, 2001] solar wind for the year 1999. (b) Cumulative distribution function for the histograms in Figure 1a. The solid line represents the probability that one would find a certain charge state larger than $\langle Q \rangle_{Fe}$ in the normal solar wind. The dashed line, corresponding to ICMEs, represents the probability that one would find an Fe charge state less than $\langle Q \rangle_{Fe}$ in a hot ICME.

comparable statistics, the normal time periods were chosen to have the same duration as those of the ICMEs. The filled histogram bars (representing normal solar wind) peak at $\langle Q \rangle_{Fe} \sim 10$, consistent with a coronal temperature around 1 MK [*Galvin and Gloeckler*, 1997; *Arnaud and Raymond*, 1992]. The unfilled bars represent hot ICME material (from the hot ICME time periods listed in Table 1 of *Lepri et al.* [2001]) and peak around $\langle Q \rangle_{Fe} \sim 12-13$. This illustrates that the ICME material identified by *Lepri et al.* [2001] is often originating from a much hotter source, as determined by $\langle Q \rangle_{Fe}$, than the normal solar wind material.

[11] Figure 1b shows the cumulative distribution function for the above histograms. The solid line corresponds to the filled histogram bars and represents the probability that one would find a certain average Fe charge state in the normal solar wind larger than the value $\langle Q \rangle_{Fe}$. The probability of finding charge states higher than 10 or 11 in the normal solar wind rapidly drops off. The dashed line represents the probability that one would find a charge state below $\langle Q \rangle_{Fe}$ in a hot ICME. As the charge states increase, they are more likely associated with ICMEs. The two curves intersect around $\langle Q \rangle_{Fe} = 11$; this value represents an equal probability that the material observed is associated with either the normal solar wind or a hot ICME. A similar crossover value was determined in examining several other years of data within the study. To further illustrate charge state distributions associated with all ICMEs, we use independently determined ICME time periods (ICME boundaries are

determined by *Cane and Richardson* [2003] (hereinafter referred to as CR)) that are associated with high Fe charge states. The ICME time periods were identified by a variety of signatures: in particular, by thorough examination of 5-min magnetic field data from the ACE magnetometer, solar wind plasma data from the Wind and ACE spacecraft, and cosmic ray intensity as measured by the anticoincidence guard of the NASA Goddard Space Flight Center (GSFC) experiment on IMP 8. Most ICME were readily identifiable on the basis of the simultaneous presence of a relatively smooth magnetic field, often with some rotation of the out-of-ecliptic component, abnormally low plasma proton temperatures, and a decrease in the cosmic ray intensity. For examples and a discussion of ICME signatures, see *Richardson and Cane* [1995] and *Cane and Richardson* [2003].

[12] The results of the survey of CR ICME versus non-ICME solar wind data are plotted in Figures 2a and 2b, similar to Figures 1a and 1b. The normal solar wind charge states are taken over the rest of the year, excluding the ICME time periods. We find that using these independently determined ICME periods for the ICME charge states results in a similar crossover value to the one obtained in Figure 1a. Once again, the peak for the normal solar wind is around $\langle Q \rangle_{Fe} = 10$. The range of charge states found within the ICME solar wind varies greatly. As I mentioned above, high Fe charge states are not observed in all ICMEs which would explain the peak around $\langle Q \rangle_{Fe} \sim 10-11$ (close to
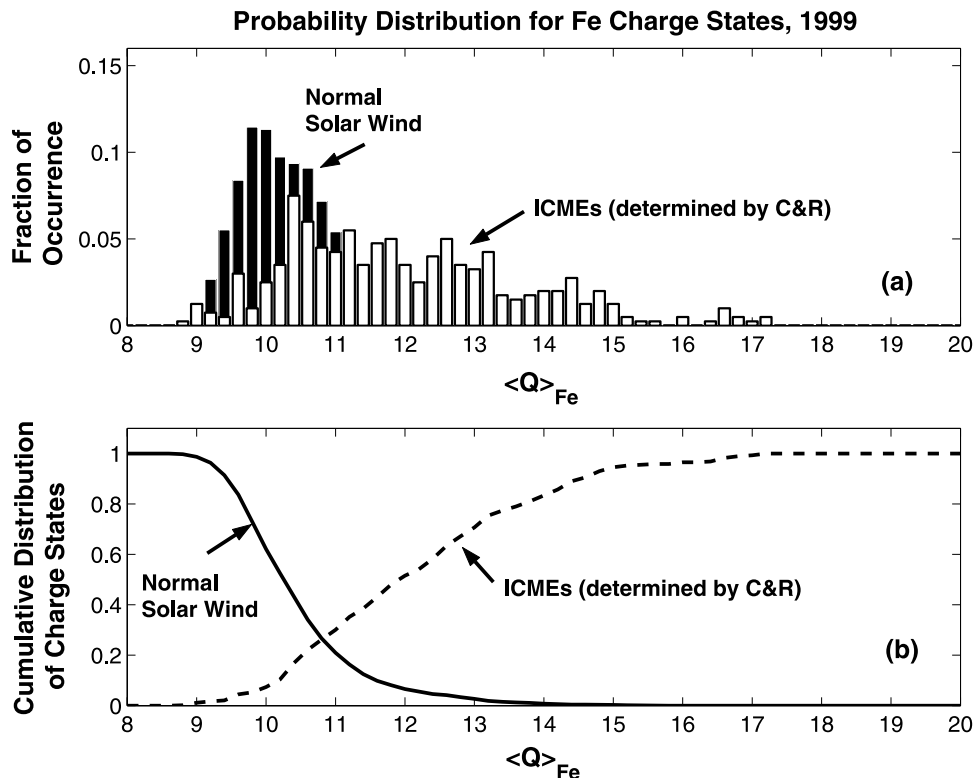
Probability Distribution for Fe Charge States, 1999

Figure 2. Similar to Figure 1, the histogram (a) represents the normalized occurrence rate of certain Fe charge states in "normal" solar wind and CR ICME solar wind. The cumulative distribution functions (b) for the histograms intersect at $\langle Q \rangle_{Fe} \sim 11.0$. This is in agreement with the crossover in Figure 1.

normal solar wind values). The majority of the data does appear at higher Fe charge states. The crossover value is still around $\langle Q \rangle_{Fe} = 11$. The charge states observed in the normal solar wind do not fall off as fast as in Figures 1a and 1b. This is likely due to the inclusion of hot ICME time periods in our data that were not found in the list of events compiled by CR, but were determined to be ICME-related by R. Skoug (private communication, 2001) through the presence of BDEs (see Table 1 of *Lepri et al.* [2001]; please note that there is no publicly available list of BDE events to use for comparison). As a result, it is probably erroneous to include these data in the normal solar wind data and their absence would therefore reduce the number of false positives at the higher charge states exhibited in the solid line representing the normal solar wind.

[13] In order to determine a threshold value of $\langle Q \rangle_{Fe}$, above which it is more likely that we have encountered ICME material rather than normal solar wind material, we choose a value that can produce false positives less than 10% of the time. We chose to set our threshold value at $\langle Q \rangle_{threshold} = 12.0$. This value is above the crossover value of $\langle Q \rangle_{Fe} = 11$ seen in both of the above comparisons. We observe negligible false positives in the hot ICME data above this threshold value, fewer than 10% of the false positives in the CR ICME data.

[14] Using our new $\langle Q \rangle_{threshold}$ criterion as a flag to identify hot ICMEs, based solely on average charge states, we sample the solar wind data from both ACE and Ulysses from 1998 to 2002. Note that this requires the high charge states to persist for only three hours, unlike the previous composition study's requirement of durations of 20+ hours.

Our study was conducted by examining five-degree intervals in Ulysses' orbital heliographic latitude. We took one of Ulysses' 5-degree-latitude intervals ($-56°$ to $-61°$ heliographic latitude), corresponding to day-of-year (DOY) 150 to 192 of 2000, and have displayed multiple solar wind parameters observed by ACE. Figure 3 shows these various solar wind parameters. Figures 3a, 3b, and 3c show proton speed V_p, temperature T_p, and density N_p from the SWEPAM instrument. In Figures 3d, 3e, and 3f, O^{7+}/O^{6+} and the Fe information are derived from the SWICS instrument. Figures 3g, 3h, and 3i contain magnetic field information from the MAG instrument. The alternating slow- and fast-speed streams (shown in the proton speed plotted in Figure 3a) are characteristic of solar maximum, with coronal hole-associated fast wind interacting with slow wind associated with closed magnetic field lines at the Sun. During this period, a number of ICMEs were observed at ACE (CR); the shaded bars running vertically through all panels denote the ICMEs. Most of the ICME time periods contain enhanced Fe charge states. The enhanced charge state data are highlighted when $\langle Q \rangle_{Fe}$ becomes greater that 12.0.

[15] Figure 4 shows $\langle Q \rangle_{Fe}$ for the same time period for ACE (Figure 4a) and Ulysses (Figure 4b). The ACE-Sun-Ulysses angle during this interval ranges from 21° on DOY 50 to 68° on DOY 130. Ulysses travels through one five-degree latitude bin, from $-21°$ to $-26°$. Due to the large separation angle, it is unlikely that Ulysses and ACE are observing material from the same source region on the Sun. The dashed lines superimposed on the panels show the $\langle Q \rangle_{threshold} = 12.0$ determined above. The increased vari-
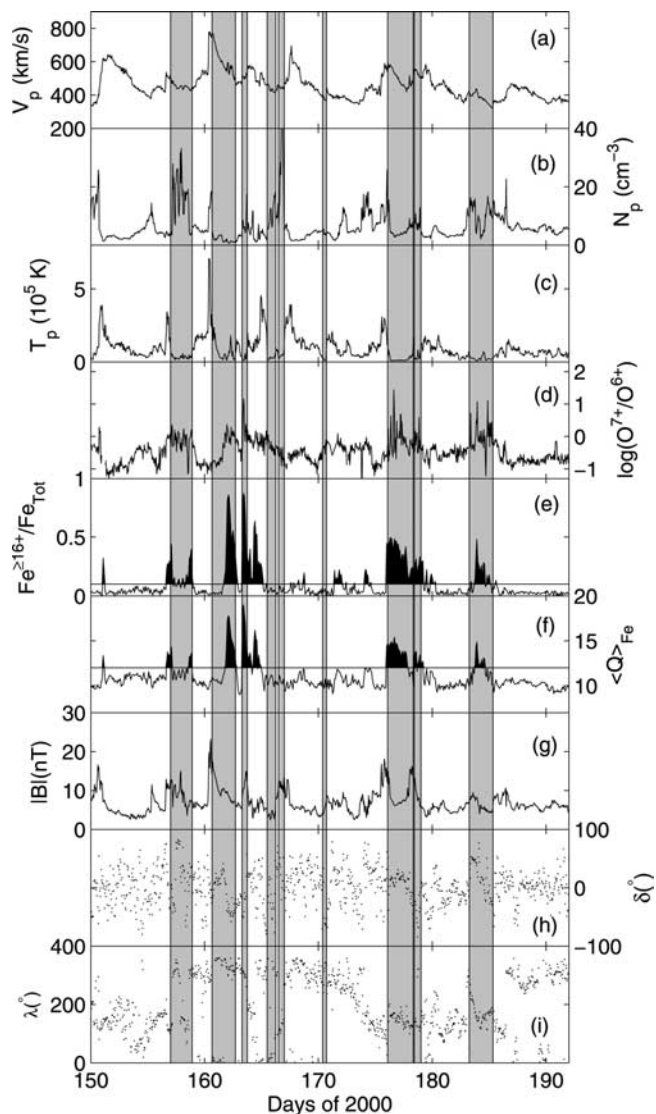
Figure 3. Summary of plasma and Fe data for DOY 150 to 192, 2000. The parameters plotted are (a) proton velocity (V_p), (b) density (N_p), (c) temperature (T_p), (d) logarithmic O^{7+}/O^{6+}, (e) high Fe charge state ratio ($Fe^{\geq 16+}/Fe_{Tot}$), (f) average Fe charge state ($\langle Q \rangle_{Fe}$), (g) magnetic field magnitude ($|B|$), (h) RTN latitude (δ), and (i) the RTN longitude (λ). ICME periods (as determined by CR) are overlaid in gray.

ability in the Ulysses data, as compared with the ACE data, can be attributed to lower counting statistics observed at larger heliocentric radii. The density of particles in the heliosphere drops rapidly as it scales as $1/R^2$. Owing to the low statistics, it is difficult to determine the physical significance of the single spikes in the Ulysses data. One can see that high average charge states attributed to hot ICMEs are observed at both in the ecliptic (ACE data), and at higher latitudes (Ulysses Data). In order to show the sensitivity of our empirical threshold, we have also included lines for ±2% (11.7, 12.3) of the threshold value of 12.0. We still catch mostly the same peaks with a small variation of the threshold value. The difference in the number of high

charge states identified at a range of latitudes is illustrated more clearly in Figure 5.

[16] Figure 5 shows the frequency at which we find $\langle Q \rangle_{Fe} \geq \langle Q \rangle_{threshold}$ within the times defined by Ulysses' 5-degree-latitude bins. The years studied encompass the ascending phase of the current solar cycle and end just before the declining phase of solar maximum. The x-markers denote how frequently charge states greater than 12.0 occur within a five-degree-latitude bin at Ulysses. The o-markers denote the frequency at which one can find high Fe charge states at ACE within the same period of time marked by the respective five-degree-latitude bin at Ulysses. Error bars are shown to illustrate the sensitivity of the threshold by looking at ±0.3 or 2.5% of the threshold value of 12.0. The upper error bars in Figure 5 represent the frequency at which $\langle Q \rangle_{Fe} \geq 11.7$. The lower error bars represent the frequency at which $\langle Q \rangle_{Fe} \geq 12.3$.

[17] The fraction of high Fe charge state events is roughly comparable between Ulysses and ACE at latitudes less than $60°$ (regions A, C, and E). In region A (which covers latitudes from $-1°$ to $-60°$) hot ICME material dominates, on average, 12% of all the data at both ACE and Ulysses. In region C (covering from $-60°$ to $+60°$ in latitude), hot ICMEs make up 13% of the data at ACE and 9% at Ulysses. In region E (from $60°$ down to $30°$), hot ICME material make up 8% of ACE data and 16% of Ulysses data. The factor of two increase in the Ulysses data might have to do with the fact that this part of the orbit is through the active latitudes (please see discussion for further comments). However, above $60°$, a clear deficit of hot ICME material is observed at Ulysses. In region B
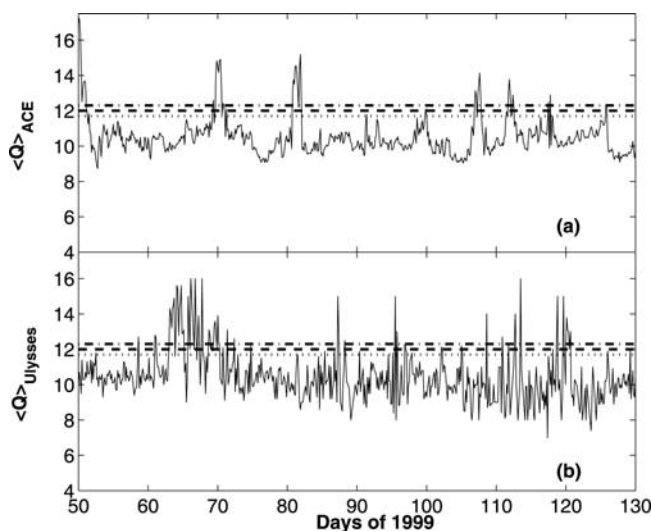

Figure 4. The average Fe charge states are shown for both ACE and Ulysses between DOY 50 and 130, 1999. The dashed line represents the threshold value of $\langle Q \rangle_{Fe} = 12.0$ that we use to identify hot ICMEs. To illustrate the sensitivity of our threshold value, we have also included lines for a variation of ±2% of the threshold value. The upper (dot-dashed line) limit is also shown at a value of $\langle Q \rangle_{Fe} = 12.3$, and the lower (dotted line) limit is shown at $\langle Q \rangle_{Fe} = 11.7$. The ACE-Sun-Ulysses angle ranges from $21°$ on DOY 50 to $68°$ on DOY 130. The heliographic latitude ranges from $-21°$ to $-26°$.
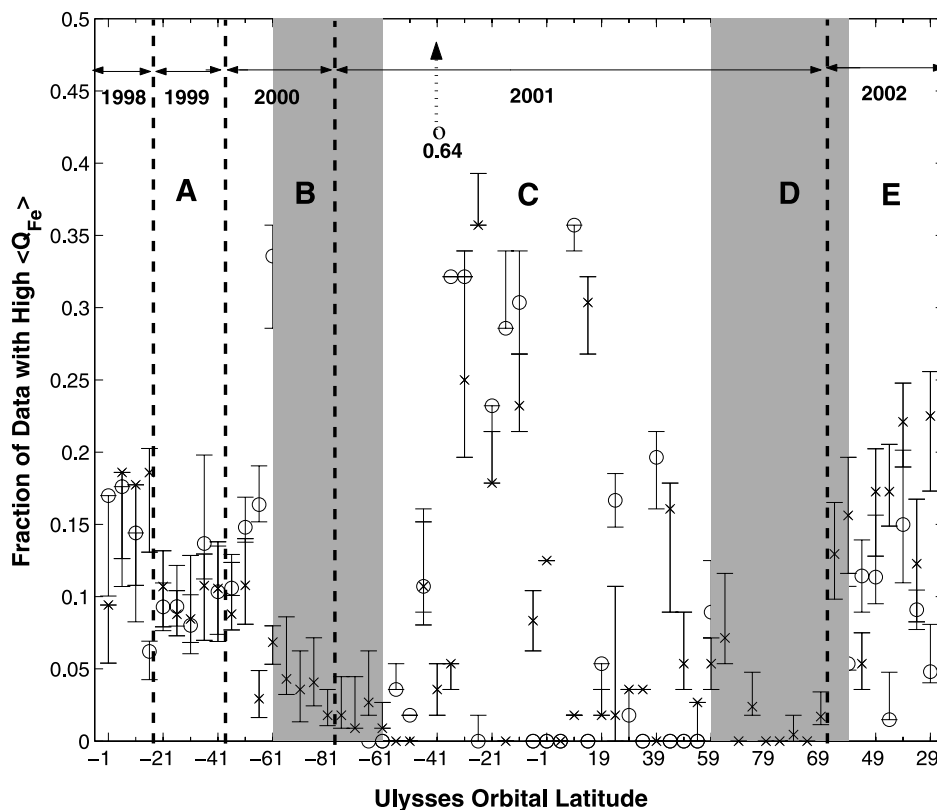
Figure 5. Frequency of events with which $\langle Q \rangle_{Fe} \geq 12.0$ in a period defined by 5°-latitude bins for Ulysses. The open circles denote the in-ecliptic ACE data. The "x" markers represent Ulysses data. Letters A through E denotes the nonshaded and shaded regions. Regions B and D represent the times when Ulysses was above 60 degrees in latitude. Notice that during these times, Ulysses observes more than an order of magnitude fewer high Fe charge states than ACE in the ecliptic. The error bars represent the sensitivity of the $\langle Q \rangle_{threshold}$ value with the upper error bar showing the fraction of data with $\langle Q_{Fe} \rangle >$ 11.7 and the lower error bar showing the fraction of data with $\langle Q_{Fe} \rangle >$ 12.3.

(at southern latitudes below 60°), the ACE data contains 13% hot ICME material (similar to the other regions), but Ulysses only contains an average of less than 4% hot ICME material, a threefold decrease from the previous latitude region and from the percentage observed at ACE. In region D (above 60° in the northern hemisphere), ACE data contains 12% hot ICME material, while Ulysses only contains less than 3% hot ICME material, down by a factor of 4 from the percentage observed at ACE. Please note that in the middle of 2001 (region C) Ulysses was going through a fast latitude sweep from negative to positive latitudes. The data bins for latitudes −51 to +49 are each composed of data from less than 10 days. The high degree of variability that exists in the data from each satellite is due to the fact that the Fe charge state enhancements may be several days long and therefore make up a majority of the data or none at all depending on where the time bins fall in relation to the high charge state events. As mentioned above, if one averages the percentage of hot ICME material observed at ACE and Ulysses during this time period, then 13% of the ACE data contains hot ICME material, and 9% of the Ulysses data contains hot ICME material. This is a deficit by a factor of 1.4, not as dramatic as the plot might make it appear. The discrep-

ancies at the high latitudes, however, remain even after the data from these time periods are averaged, as mentioned above. The high-latitude data contain on average over 1/3 less hot ICME material than is observed in the ecliptic. *Gosling et al.* [1993] implied that according to BDE data, ICME signatures are seen in about 15% of all solar wind data observed near solar maximum. We obtain similar results in the in-ecliptic ACE data if we average our fractions over 1 year in accordance with their methods. However, the Ulysses data breaks from this trend while at high latitudes.

[18] Figure 6 shows the monthly averaged sunspot number reported by the Sunspot Index Data Center (available at http://sidc.oma.be). Overlaid on this plot are two time periods that correspond to regions B and D from Figure 5. The data from this study cover the ascending phase of the current solar cycle up until just before the declining phase. The data from the high latitudes show a clear deficit in hot ICME material regardless of the fact that these time periods occur right at solar maximum. Although the Sun's activity is at its maximum, the phenomena that produce high Fe charge states are governed more by latitude than by solar activity. It appears that the latitudinal effects far outweigh the solar cycle
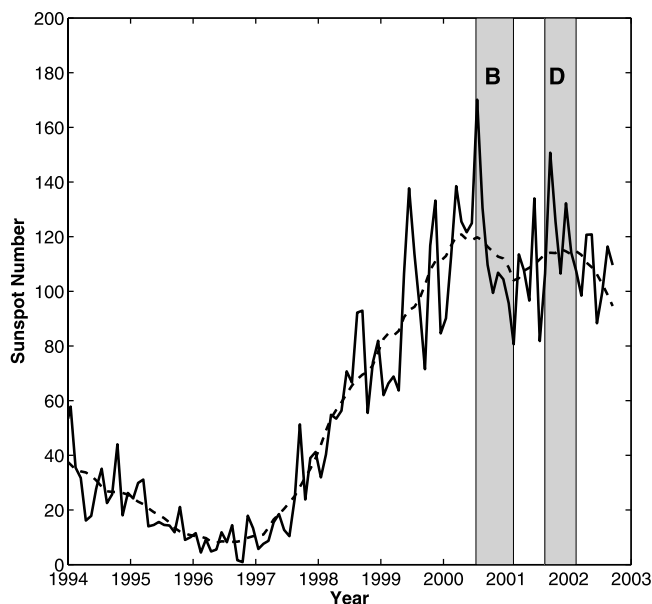
Figure 6. Monthly sunspot numbers (solid line) and monthly smoothed sunspot numbers (dashed line) for the years 1994 to 2003 (from the SIDC, RWC). Our study encompasses the ascending phase of the current solar cycle to just before the declining phase. The shaded regions marked B and D represent the times when Ulysses was at latitudes beyond 60°. Although these excursions to high latitude were during maximum solar activity levels, the number of observed high Fe charge states dropped off substantially at Ulysses (refer also to Figure 5.).

effects resulting in decreased occurrence rates of hot ICMEs.

4. Discussion

[19] In order to begin to understand why the high Fe charge states occur more frequently at lower latitudes, one needs to first consider the physical processes that produce the observed charge states. What scenarios produce coronal electron temperatures high enough to ionize Fe atoms to such a high degree (at these energies, photoionization is not important at coronal densities and photon fluxes [*Hundhausen*, 1972]) and what processes feed them into the solar wind, preserving their high charge states, allowing them to be observed by in situ satellites? The scenario proposed to answer these questions must simultaneously be able to describe the observed latitudinal dependence in the occurrence rate of high Fe charge states.

[20] Let us start by examining latitudinal considerations on the Sun through the solar cycle. The solar magnetic fields vary throughout the solar cycle; the field is mostly dipolar at solar minimum and becomes more complicated with no clear latitudinal ordering as solar maximum approaches. At solar minimum, the current sheet, which separates the opposite polarity global magnetic fields into two hemispheres, is located near the solar equator and originates above the cusps of the helmet streamers. As the solar magnetic fields evolve toward solar maximum conditions, the current sheet becomes increasingly warped and

highly inclined with respect to the solar equator. The coronal helmet streamers are no longer confined to the equator, but appear at larger latitudes as well [*Gibson*, 2001]. In 1998, at the start of our study, the streamer belt was essentially a wide band centered near the equator. It extended in latitude up to 45 degrees at this point. By 1999, there was no longer a simple belt structure and the current sheet was becoming highly warped. By the time solar maximum arrived in 2000, streamers were found at a wide range of latitudes, extending up to the poles. The magnetic field was evolving toward a quadrupolar configuration.

[21] In general, we know that CMEs are associated with large-scale closed magnetic field regions on the Sun [*Hundhausen*, 1993]. There are two types of large-scale closed field regions in the solar corona; one is the "bipolar" helmet streamer, found to occur between coronal holes with opposite polarity, the other is the so-called "unipolar" helmet streamer that occurs between two like-polarity open field regions [*Zhao and Webb*, 2003; *Hundhausen*, 1972]. The majority of CMEs ($\sim$75%) originate from closed fields from preexisting bipolar coronal streamers [*Zhao and Webb*, 2003; *Webb et al.*, 1994]. It has been previously reported that during solar maximum, CMEs are distributed over a broad range of apparent latitudes [*Hundhausen*, 1993]. This is consistent with the fact that the streamer belt becomes distorted and extends to high latitudes during enhanced solar activity. Recent CME time-latitude distribution plots indicate that increased solar activity does indeed lead to numerous CMEs observed at high latitudes [*Pojoga and Huang*, 2002]. However, latitudinal studies over the period of 1984–1989 from the SMM mission [*Burkepile and St. Cyr*, 1993; *Hundhausen*, 1993] show that there are still fewer CMEs observed in the polar regions during the climax of solar activity.

[22] In addition to understanding how the global magnetic field influences solar phenomena, we must also specifically concentrate on the phenomena capable of creating the environment to highly ionize Fe atoms. Knowledge of the physical processes responsible for creating these high charge states is necessary to fully understand their observed latitudinal distribution. Let us start by examining the average charge state of Fe. In order to produce an average charge state of 12.0, the sample material must contain Fe ions with a range of charges, some more than Q = 12.0 and some less than Q = 12.0. Looking at the charge state distributions (as we did in our 2001 study), we see that there are many ions with charge states up to and above Q = 16. In order to produce a charge state of Fe^{16+} the surrounding material must be at temperatures around 5 MK. Depending on the expansion speed, Fe charge states freeze in over a range of solar radii; this implies that the temperatures inferred from the charge states are most likely a lower limit of surrounding material's temperature. That means that coronal temperatures in excess of 5MK are needed to produce the highest Fe charge states we observe. The only phenomena that exist that are capable of creating enough energy to ionize the surrounding material to such extreme temperatures are solar flares.

[23] Solar flares are known to be capable of creating extreme temperatures in excess of 10 MK. In the initial stages of a flare, a prominence, or filament, and its overlying arcade that have been present for several days undergo a
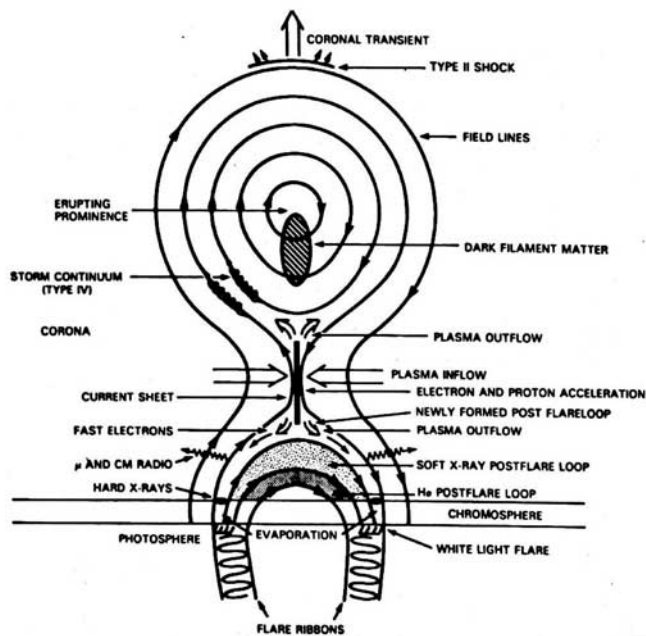
Figure 7. The global structure of the classic two-ribbon flare model showing the location of the major energy conversion processes. Note that plasma flows into the reconnection region (where the current sheet is produced) where the electrons are accelerated and subsequently flow out into both the post-flare loop and into the erupting prominence and related magnetic flux rope. This is a cross sectional view along the neutral line (adapted from *Martens and Kuin* [1989]).

sudden loss in equilibrium. This nonequilibrium triggers the eruption; the prominence begins to lift off, stretching the surrounding arcade magnetic fields lines as it rises. Beneath the prominence, an evacuated region is left behind and the remaining stretched field lines begin to move together to form a thin current sheet. The eruption cannot proceed unless reconnection acts to dissipate the newly formed current sheet [*Roussev et al.*, 2003]. As the field lines beneath the flux rope are brought together, they begin to reconnect, releasing a vast amount of energy ($10^{28}-10^{34}$ ergs) over a time scale of minutes to hours [*Kivelson and Russell*, 1995; *Carroll and Ostlie*, 1996, and references therein]. As this reconnection proceeds, the prominence erupts increasing the rate of reconnection due to the increased magnetic gradients caused by the stretching of the field lines [*Haisch et al.*, 1991]. Refer to Figure 7 for an illustration of the classical two-ribbon flare eruption scenario [*Martens and Kuin*, 1989]. Observations show that particles (particularly electrons) are accelerated in large numbers to high energies in the reconnection region [*Jakimiec*, 2002]. Although the true nature of the particle acceleration in flares is not known, the main theories and models to explain it are direct acceleration through the diffusion region [*Øieroset et al.*, 2001], DC electric field acceleration [*Tsuneta*, 1985, 1995; *Holman*, 1985; *Litvinenko*, 1996], stochastic acceleration through wave-particle interaction [*Miller*, 1991; *Miller and Viñas*, 1993; *Miller and Roberts*, 1995; *Miller et al.*, 1996; *Miller*, 1997; *Aschwanden*, 1999], and shock acceleration [*Somov and*

Kosugi, 1997; *Tsuneta and Naito*, 1998; *Somov et al.*, 1999; *Masuda et al.*, 1994]. In the reconnection region, both the resulting heated material and accelerated particles flow out either into the post flare loop or into the rising flux rope [*Haisch et al.*, 1991; *Martens and Kuin*, 1989]. The high-energy electrons will subsequently ionize the surrounding material as long as the ionization time scale is shorter than the expansion time scale (until the freeze-in point for the material expanding away from the solar surface) or until an equilibrium is reached and the energy is dissipated (such as in the post flare loop) [*Kivelson and Russell*, 1995; *Priest and Forbes*, 2002]. It is in this region where the highly ionize Fe is produced either by direct heating in the reconnection region or by electron collisions, the latter playing the dominant role. It has been modeled that this beam is responsible for the observed charge states up to 20+ in energetic Fe [*Miller and Viñas*, 1993]. This electron beam may also be capable of ionizing the bulk plasma along with thermal Fe. The elevated charge states may relax somewhat out to the freeze-in location. However, the beam also heats the plasma, causing a more rapid expansion of the plasma; this may slow the relaxation time, preserving the high charge states. We propose this mechanism as being responsible for the creation of the high Fe charge states observed by ACE and Ulysses.

[24] The question still remains as to how the heated Fe makes it into the CME? *Richardson et al.* [2003] found that out of 22 ICME events with $\langle Q \rangle_{Fe} > 14.0$, 10 of the high charge state ICMEs have clear associations with solar flares (C7-X6), eight have probable associations, one was associated with a LASCO halo CME with no reported flare, and the other two events had unclear associations. These results lend credence to the idea that flaring regions are capable of producing the high charge states we observe. Since our criteria are less strict ($\langle Q \rangle_{Fe} > 12.0$), we conducted our own survey of hot ICME events.

[25] In order to provide observational evidence for the scenario proposed above, we examined a subset of the ACE data in detail. Please note that for this portion of the study, we are only examining high Q_{Fe} in the ecliptic. From the CR ICME list, we selected ICMEs that had an associated LASCO CME. Using these ICMEs we are able to investigate features on the Sun that may tell us about the origins of the high Fe charge states. For each CR ICME, we have Fe charge state data. We examined the combined EIT and C2 movies from the SOHO/LASCO CME Catalog (available at http://cdaw.gsfc.nasa.gov/CME_list/UNIVERSAL/). This CME catalog is generated and maintained by the Center for Solar Physics and Space Weather, Catholic University of America, in cooperation with the Naval Research Laboratory and NASA. The subsequent study was limited to periods that had all of the following data available: Q_{Fe} data, ICME listings in CR, LASCO CME associations, and EIT (195 Å) and C2 movies. In addition, we also used the Solar Event Reports (available at http://solar.sec.noaa.gov/ftpmenu/indices.html) provided by the Space Environment Center, a division of the National Oceanic and Atmospheric Administration, to determine the solar features catalogued and to verify the temporal relevance of these features. In all, there were 57 epochs that fit our criteria from the years 1998 (beginning 6 February) to the end of 2001. As stated above, these 57 events were simultaneously identified by helio-

Table 1. Results of the Study of Coronal Features Associated With 57 CMEs on the Sun

Coronal Feature	Yes	No
$\langle Q \rangle_{Fe} > 12.0$	75%	25%
EIT Disturbance	95%	93%
Near Central Meridian	98%	29%
Near Limb	2%	71%
Flare Association in SER.	76%	100%
Flare Class: B	3%	8%
C	35.5%	23%
M	35.5%	38%
X	26%	31%

spheric and coronagraph observations. The characteristics of the epochs are summarized in Table 1.

[26] Of the 57 events studied, 43 (or 75%) of them exhibited at least 6 consecutive hours of $Q_{Fe} > 12.0$. The rest, 14 (or 25%), did not have $Q_{Fe} > 12.0$ for at least 6 consecutive hours. For each of these epochs, we examined the C2/EIT movies for eruptions occurring near the time of the CME (as listed by the LASCO catalog). Figure 8 shows an example of the time lapsed C2 and EIT movie for the halo CME on 29 March 2001. For this example, a LASCO CME was listed as occurring at 1026 UT. It is hard to see the coronal features of the CME in these images. A superimposed circle is drawn on each frame to mark the region where a flare occurred near the time of the CME. In Figure 8a, the marked region shows general brightening characteristic of active regions. In Figure 8b, there is a distinct brightening in the circle; notice that this image was taken 2 min before the CME was observed in the C2 image that marks the start time. This brightening continues in Figures 8c and starts to fade in Figure 8d. The flare is described in the SEC's Solar Event Reports. The GOES 8 satellite recorded a start time of 0957 UT, peaking at 1015 UT and ending at 1032 UT. The flare is listed as an X-class flare. It is in this way that we determined an association of flares with CMEs. We require a flare to occur within 1 hour (as listed in the SEC's SER) of the LASCO CME time, and look for erupting features in the EIT images. For the high Q_{Fe} events, 41 (95%) show a disturbance on the disc of the Sun occurring near the time of the CME. Of the 41, all but one have disturbances occurring near the central meridian of the Sun, the other occurred near the limb near where the CME appears to originate.

[27] Of the 14 without high Q_{Fe}, 13 (93%) are associated with an EIT disturbance. The differentiating characteristics are that of those associated with an EIT disturbance, 10 (71%) occur near the limb (in the outer 30% of the disc) and three (29%) occur closer to the central meridian. This highlights that the major difference in observable features of the two cases (with high Q_{Fe}, and without high Q_{Fe}) is where on the disk the flare occurs. If the flare is near the limb, it is less likely that the heated material and the accelerated electrons are going to contribute the parts of the ICME we observe at Earth.

[28] Let us further examine the data set. For the 41 epochs with $Q_{Fe} > 12.0$ that display an EIT disturbance, 31 (76%) have an associated flare (occurring within an hour of the LASCO CME time) listed in the SER. Of these 31 events, the breakdown by flare type is as follows: 3% are type B, 35.5% are type C, 35.5% are type M, and 26% are type X

flares. Of the 13 without $Q_{Fe} > 12.0$, but with EIT associated disturbances, all (100%) have associated flares listed in the SER. The breakdown by type is as follows: 8% are type B, 23% are type C, 38% are type M, and 31% are type X. Therefore there does not appear to be any correlation of flare size with whether or not an ICME will exhibit $Q_{Fe} > 12.0$.

[29] In a recent survey of LASCO CMEs from 1997 to 2001 [*Zhou et al.*, 2003], it was reported that 88% of halo CMEs were associated with flares. These flares have the ability to heat the surrounding plasma and accelerate electrons to energies higher than the upper stage ionization energies for many heavy ions, including Fe. Flares are the only solar phenomenon that occur with enough frequency and are able to create hot enough electrons to produce these high Fe ionization states that persist for hours to days. In order to be able to observe this flare heated material in the heliosphere, a CME must occur near the time and location of the flare, providing the magnetic connection to the CME magnetic fields that eventually are dragged outward into the heliosphere. If, for some reason, no magnetic connectivity exists between the flare site and the CME, then the high energy electrons and heated plasma have no way of making it onto a field line in an ICME.

[30] The lack of high Q_{Fe} in ICME where flares are seen to occur near the limb may imply that these regions are not magnetically connected to the parts of the ICME field lines
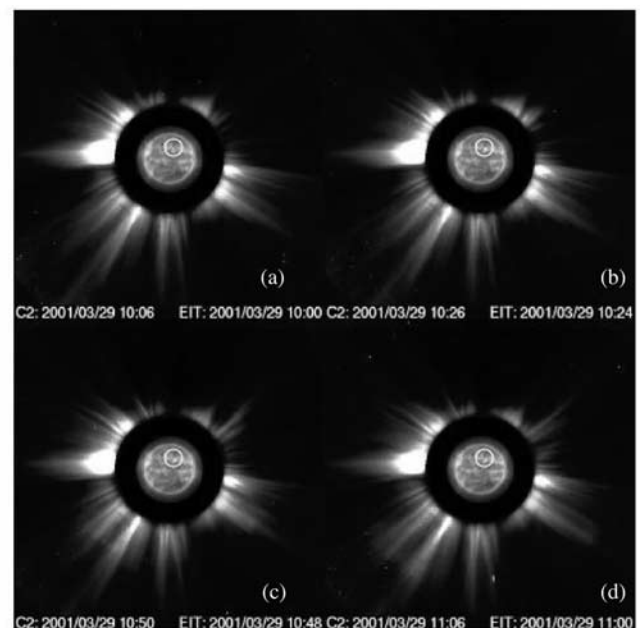

C2: 2001/03/29 10:06   EIT: 2001/03/29 10:00   C2: 2001/03/29 10:26   EIT: 2001/03/29 10:24

C2: 2001/03/29 10:50   EIT: 2001/03/29 10:48   C2: 2001/03/29 11:06   EIT: 2001/03/29 11:00

Figure 8. Time series image from combined LASCO C2 and EIT images for a halo CME occurring 29 March 2001. The superimposed circular region in all the panels represents the area where brightening occurred in association with the CME. (a) The marked regions shows brightening characteristic of active regions at 195 Å. (b) The a brightening can be seen in the marked circle just two minutes before the CME was observed in the C2 image. The brightening lasts into Figure 8c and begins to fade in Figure 8d. Images are courtesy the SOHO/LASCO CME catalog.

that expand out and pass the spacecraft at L1. The above scenario seems to support the observations of high Q_{Fe} in ICME material originating within a few tens of degrees of the flaring region. It also provides reasoning for the lack of high Q_{Fe} in all ICMEs, especially those without associated flares or those associated with flares on the limbs. The nonubiquitous occurrence of high Q_{Fe} is most likely due to the fact that magnetic fields in the corona can be highly complex and may not always provide a direct connection between the flare plasma and the ICME field lines and/or that not all parts of an ICME connect to the same region on the Sun.

[31] The above description illustrates why enhanced Fe charge states may and may not be observed in the ecliptic during ICME time periods. We will now address why there is an observe deficit in the number of high-latitude, high Fe charge states based on the assumption that flare-ionized material is picked up by CMEs as they erupt. Flares erupt from magnetically active regions around sunspot groups characterized by increased magnetic field strength and complexity. Flares originate from active region latitudes; these form at midlatitudes ($\sim 30°$) and migrate toward the equator as the solar cycle progresses [*Hundhausen*, 1993]. Their quantities, and therefore flare occurrences, track the solar cycle. As a result, the incidence of flares is highest near solar maximum and most are located within $\sim \pm 30°$ of the solar equator [*Behr and Siedentopf*, 1952; *Ramanathan*, 1962]. If we examine distribution of flares on the Sun during our study from 1998 to 2002 [*Pojoga and Huang*, 2002], we can see that they start out at higher latitudes at the beginning of the solar cycle and then spread equatorward. However, even as they are spreading equatorward, many flares are still occurring at higher latitudes. There were a couple of flares occurring at latitudes up to 40 degrees in 2000 and 2001 [*Pojoga and Huang*, 2002]. Since the average extent of a CME is 40 degrees and may have widths up to 120 degrees, it is possible that a CME launched from active latitudes could grab the flare material and spread it out over a very large angular extent [*Hundhausen*, 1993]. It can be inferred from *Pojoga and Huang*'s [2002] data that flares near 40 degrees do not happen with the same frequency as lower-latitude flares. And, because most CMEs extend over 40 degrees in latitude, it would make sense that CME originating near a flaring region may not have enough angular width to carry the material to high latitudes. In general, high-latitude CMEs have been reported to occur with lower frequency than their lower-latitude counterparts [*Burkepile and St. Cyr*, 1993; *Hundhausen*, 1993]. Also, many high-latitude CMEs are associated with polar crown filament eruptions originating from cooler regions and would therefore not contain the hot material we observe. The CMEs occurring at high latitudes may not always be magnetically connected to flares at lower latitudes. Hence, since flares occur at lower latitudes and because flare material can only enter the solar wind when magnetically connected (e.g., during coronal mass ejections), it follows that there would be less flare heated material observed in situ at higher latitudes. However, a nonzero number of high Fe charge states have been observed at high latitudes. In this case, Ulysses observations of high Q_{Fe} above $\pm 60°$ may be due to passage through flare-associated, high-latitude ICMEs that are well separated from the flaring regions. The presence of flare material at high latitudes may be explained by mechanisms such as those in *Odstrcil and Pizzo*'s [1999a, 1999b] simulations. In their simulation, a CME is launched from low or middle latitudes and distorted by plasma interactions, becoming pancake-like and extended in latitude. These plasma interactions may be responsible for transporting hot material created at low or middle latitudes up into the higher latitudes.

5. Summary

[32] We conclude that flares have the capability of ionizing Fe in the bulk loop plasma to unusually high charge states. The electron beam created at the reconnection site during a flare will deposit high-energy electrons both into the post flare loop and into the expanding prominence and surrounding flux rope. The high-energy electrons will subsequently interact with the plasma producing high charge states. Reconnection will also heat the surrounding plasma, causing a more rapid expansion and allowing the high charge states to be preserved as the flux rope expands. If a CME erupts near in time and space to the flaring region and a magnetic connection is established between the two phenomena, the heated material can become a substantial part of the CME and be carried out with the ejecta into the heliosphere.

[33] In the study of CR ICMEs associated with a LASCO CME, we found that 95% of ICMEs with high Fe charge states at ACE (hot ICMEs) were associated with an EIT disturbance near the time of the CME. Of the 95% of hot ICMEs associated an EIT disturbance, 98% had disturbances that occurred near the central meridian. In contrast, the ICMEs not associated with high Fe charge states had a 93% correlation with EIT disturbances, with only 29% occurring near the central meridian. Although both the ICMEs with and without high Fe charge states had high correlation with flares from the Solar Event Reports and with EIT disturbances, the major differentiating factor is where on the disc of the Sun these disturbances occur with respect to the observing satellite. This leads us to the conclusion that magnetic connectivity of the part of the ICME observed in situ to a flaring region is the key to whether or not high Fe charge states will be present.

[34] The lack of high-latitude hot ICMEs can be explained if the high Fe charge states are created in flares and are therefore confined to the active latitudes. The occasional observation of high Fe charge states at high latitudes is most likely a result of either direct magnetic connection of the high latitude ICME to lower, active latitudes on the Sun, or plasma interactions which cause the ICME to distort as it travels away from the Sun, becoming extended in latitude. The fact that not all ICMEs exhibit high Fe charge states may be due either to the fact that there is no magnetic connection to a flaring region, thereby not providing a path for the highly ionized Fe to enter the CME, or by the absence of a flare near the time that the CME occurs. In the future, we plan to further investigate flare heating as the source of the observed high charge states of heavy ions using different flare and CME models.

References

Antiochos, S. K. (1998), The magnetic topology of solar eruptions, *Astrophys. J.*, *502*, 181.

Arnaud, M., and J. Raymond (1992), Iron ionization and recombination rates and ionization equilibrium, *Astrophys. J.*, *398*, 394.

Aschwanden, M. J. (1999), Particle acceleration and kinematics in solar flares and the solar corona, in *Magnetic Fields and Solar Processes, Proceedings of the 9th European Meeting on Solar Physics*, edited by A. Wilson, pp. 1015, Eur. Space Agency, Noordwijk, Netherlands.

Bame, S. J., J. R. Asbridge, W. C. Feldman, and P. D. Kearney (1974), The quiet corona: Temperature and temperature gradient, *Sol. Phys.*, *35*, 137.

Behr, A., and H. Siedentopf (1952), Zur Statistik von Sonneneruptionen. Mit 6 Textabbildungen, *Zeitschrift Astrophys.*, *30*, 177.

Borrini, G., J. T. Gosling, S. J. Bame, and W. C. Feldman (1982), Helium abundance enhancements in the solar wind, *J. Geophys. Res.*, *87*, 7370.

Bürgi, A., and J. Geiss (1986), Helium and minor ions in the corona and solar wind—Dynamics and charge states, *Sol. Phys.*, *103*, 347.

Burkepile, J. T., and O. C. St. Cyr (1993), A revised and expanded catalogue of mass ejections observed by the Solar Maximum Mission coronagraph, *Tech. Note NCAR/TN-367+STR*, Natl. Cent. for Atmos. Res., Boulder, Colo.

Burlaga, L. F. (1991), Magnetic clouds, in *Physics of the Inner Heliosphere*, vol. 2, p 1–22, Springer-Verlag, New York.

Cane, H. V., and I. G. Richardson (2003), Interplanetary coronal mass ejections in the near-Earth solar wind during 1996–2002, *J. Geophys. Res.*, *108*(A4), 1156, doi:10.1029/2002JA009817.

Carroll, B. W. and D. A. Ostlie (1996), *An Introduction to Astrophysics*, Addison-Wesley, Reading, Mass.

Fenimore, E. E. (1980), Solar wind flows associated with hot heavy ions, *Astrophys. J.*, *235*, 245.

Galvin, A. and G. Gloeckler (1997), Charge state composition in coronal hole and CME related solar wind: Latitudinal variations observed by Ulysses and Wind, in *Correlated Phenomena at the Sun, in the Heliosphere and in Geospace*, edited by A. Wilson, p. 323, Eur. Space Agency, Noordwijk, Netherlands.

Gibson, S. E. (2001), Global solar wind structure from solar minimum to solar maximum: Sources and evolution, *Space Sci. Rev.*, *97*, 69.

Gloeckler, G., et al. (1992), The Solar Wind Ion Composition Spectrometer, *Astron. Astrophys. Suppl. Ser.*, *92*, 267.

Gloeckler, G., et al. (1998), Investigation of the composition of solar and interstellar matter using solar wind and pickup ion measurements with SWICS and SWIMS on the ACE spacecraft, *Space Sci. Rev.*, *86*, 495.

Gloeckler, G., et al. (1999), Unusual composition of the solar wind in the 2–3 May 1998 CME observed with SWICS on ACE, *Geophys. Res. Lett.*, *26*, 157.

Gosling, J. T. (1990), Coronal mass ejections and magnetic flux ropes in interplanetary space, in *Physics of Magnetic Flux Ropes*, *Geophys. Monogr. Ser.*, vol. 58, edited by C. T. Russell, E. R. Priest, and L. C. Lee, p. 343, AGU, Washington, D.C.

Gosling, J. T., and P. Riley (1996), The acceleration of slow coronal mass ejections in the high-speed solar wind, *Geophys. Res. Lett.*, *23*, 2867.

Gosling, J. T., S. J. Bame, W. C. Feldman, D. J. McComas, J. L. Phillips, and B. E. Goldstein (1993), Counter-streaming suprathermal electron events upstream of corotating stream interaction regions: Ulysses, *Geophys. Res. Lett.*, *20*, 2789.

Haggerty, D. K., et al. (2000), Acceleration and transport of energetic particles observed in the heliosphere, *AIP Conf. Proc.*, *528*, 266.

Haisch, B., K. T. Strong, and M. Rodonò (1991), Flares on the Sun and other stars, *Annu. Rev. Astron. Astrophys.*, *29*, 275.

Henke, T., et al. (1998), Differences in the O^7/O^6 ratio in magnetic cloud and non-cloud coronal mass ejections, *Geophys. Res. Lett.*, *25*, 3465.

Holman, G. D. (1985), Acceleration of runaway electrons and Joule heating in solar flares, *Astrophys. J.*, *293*, 584.

Hundhausen, A. J. (1972), *Coronal Expansion and Solar Wind*, Springer-Verlag, New York.

Hundhausen, A. J. (1993), Sizes and locations of coronal mass ejections: SMM observations from 1980 and 1984–1989, *J. Geophys. Res.*, *98*, 13,177.

Jakimiec, J. (2002), A new model of electron acceleration in solar flares, in *Solar Variability: From Core to Outer Frontiers, Proceedings of the 10th European Solar Physics Meeting*, edited by A. Wilson, p. 645, Eur. Space Agency, Noordwijk, Netherlands.

Kivelson, M. G. and C. T. Russell (1995), *Introduction to Space Physics*, Cambridge Univ. Press, New York.

Lepri, S. T., T. H. Zurbuchen, L. A. Fisk, I. G. Richardson, H. V. Cane, and G. Gloeckler (2001), Fe charge distributions as an identifier of interplanetary coronal mass ejections, *J. Geophys. Res.*, *106*, 29,231.

Litvinenko, Y. E. (1996), Particle acceleration in reconnecting current sheets with a nonzero magnetic field, *Astrophys. J.*, *462*, 997.

Martens, P. C. H., and N. P. M. Kuin (1989), A circuit model for filament eruptions and two-ribbon flares, *Sol. Phys.*, *122*, 263.

Masuda, S., T. Kosugi, H. Hara, S. Tsuneta, and Y. Ogawara (1994), A loop-top hard X-ray source in a compact solar flare as evidence for magnetic reconnection, *Nature*, *371*, 495.

McComas, D. J., R. Goldstein, J. T. Gosling, and R. M. Skoug (2001), Ulysses' second orbit: Remarkably different solar wind, *Space. Sci. Rev.*, *97*, 99.

Miller, J. A. (1991), Magnetohydrodynamic turbulence dissipation and stochastic proton acceleration in solar flares, *Astrophys. J.*, *376*, 342.

Miller, J. A. (1997), Electron acceleration in solar flares by fast mode waves: Quasi-linear theory and pitch-angle scattering, *Astrophys. J.*, *491*, 939.

Miller, J. A., and D. A. Roberts (1995), Stochastic proton acceleration by cascading Alfven waves in impulsive solar flares, *Astrophys. J.*, *452*, 912.

Miller, J. A., and A. F. Viñas (1993), Ion acceleration and abundance enhancements by electron beam instabilities in impulsive solar flares, *Astrophys. J.*, *412*, 386.

Miller, J. A., T. N. La Rosa, and R. L. Moore (1996), Stochastic electron acceleration by cascading fast mode waves in impulsive solar flares, *Astrophys. J.*, *461*, 445.

Neugebauer, M., R. Goldstein, and B. E. Goldstein (1997), Features observed in the trailing regions of interplanetary clouds from coronal mass ejections, *J. Geophys. Res.*, *102*, 19,743.

Odstrcil, D., and V. J. Pizzo (1999a), Three-dimensional propagation of CMEs in a structured solar wind flow: 1. CME launched within the streamer belt, *J. Geophys. Res.*, *104*, 483.

Odstrcil, D., and V. J. Pizzo (1999b), Three-dimensional propagation of coronal mass ejections in a structured solar wind flow: 2. CME launched adjacent to the streamer belt, *J. Geophys. Res.*, *104*, 493.

Øieroset, M., T. D. Phan, M. Fujimoto, R. P. Lin, and R. P. Lepping (2001), In situ detection of collisionless reconnection in the Earth's magnetotail, *Nature*, *412*, 414.

Owocki, S. P., T. E. Holzer, and A. J. Hundhausen (1983), The solar wind ionization state as a coronal temperature diagnostic, *Astrophys. J.*, *275*, 354.

Pojoga, S., and T. S. Huang (2002), On the sudden disappearances of solar filaments and their relationship with coronal mass ejections, *Am. Astron. Soc. Conf. Proc.*, *200*, 3714.

Priest, E. R., and T. G. Forbes (2002), The magnetic nature of solar flares, *Astron. Astrophys. Rev.*, *10*, 313.

Ramanathan, A. S. (1962), Distribution of sunspots in heliographic latitude, *Observatory*, *82*, 254.

Reinard, A. A., T. H. Zurbuchen, L. A. Fisk, S. T. Lepri, R. M. Skoug, and G. Gloeckler (2001), Comparison between average charge states and abundances of ions in CMEs and the slow solar wind, *Am. Inst. Phys. Conf. Proc.*, *598*, 139.

Richardson, I. G., and H. V. Cane (1995), Regions of abnormally low proton temperatures in the solar wind (1965–1991) and their association with ejecta, *J. Geophys. Res.*, *100*, 23,397.

Richardson, I. G., H. V. Cane, S. T. Lepri, T. H. Zurbuchen, and J. T. Gosling (2003), Spatial relationship of signatures of interplanetary coronal mass ejections, in *Solar Wind Ten*, edited by M. Velli et al., *AIP Conf. Proc., 679*.

Roussev, I. I., T. G. Forbes, T. I. Gombosi, I. V. Sokolov, D. L. DeZeeuw, and J. Birn (2003), A three-dimensional flux rope model for coronal mass ejections based on a loss of equilibrium, *Astrophys. J.*, *588*, L45.

Skoug, R. M., W. C. Feldman, J. T. Gosling, D. J. McComas, D. B. Reisenfeld, C. W. Smith, R. P. Lepping, and A. Balogh (2000), Radial variation of solar wind electrons inside a magnetic cloud observed at 1 and 5 AU, *J. Geophys. Res.*, *105*, 27,269.

Somov, B. V., and T. Kosugi (1997), Collisionless reconnection and high-energy particle acceleration in solar flares, *Astrophys. J.*, *485*, 859.

Somov, B. V., E. Y. Merenkova, T. Kosugi, T. Sakao, S. Masuda, and A. V. Oreshina (1999), Three-dimensional reconnection in the solar corona related to Yohkoh observations, in *Magnetic Fields and Solar Processes,*

Proceedings of the 9th European Meeting on Solar Physics, edited by A. Wilson, Eur. Space Agency, Noordwijk, Netherlands.

Tsuneta, G. D. (1985), Heating and acceleration processes in hot thermal and impulsive solar flares, *Astrophys. J. Lett.*, *290*, 353.

Tsuneta, G. D. (1995), Particle acceleration and magnetic reconnection in solar flares, *Publ. Astron. Soc. Jpn.*, *47*, 691.

Tsuneta, G. D., and T. Naito (1998), Fermi acceleration at the fast shock in a solar flare and the impulsive loop-top hard X-ray source, *Astrophys. J.*, *495*, L67.

von Steiger, R., N. A. Schwadron, L. A. Fisk, J. Geiss, G. Gloeckler, S. Hefti, B. Wilken, R. F. Wimmer-Schweingruber, and T. H. Zurbuchen (2000), Composition of quasi-stationary solar wind flows from Ulysses/ Solar Wind Ion Composition Spectrometer, *J. Geophys. Res.*, *105*, 27,217.

Webb, D. F., and R. A. Howard (1994), The solar cycle variation of coronal mass ejections and the solar wind mass flux, *J. Geophys. Res.*, *99*, 4201.

Webb, D. F., T. G. Forbes, H. Aurass, J. Chen, P. Martens, B. Rompolt, V. Rusin, S. F. Martin, and V. Gaizauskas (1994), Material ejection, *Solar Phys.*, *153*, 73.

Zhao, X. P., and D. F. Webb (2003), Source regions and storm effectiveness of frontside full halo coronal mass ejections, *J. Geophys. Res.*, *108*, 1234.

Zhou, G., J. Wang, and Z. Cao (2003), Correlation between halo coronal mass ejections and solar surface activity, *Astron. Astrophys.*, *397*, 1057.

—————————————

S. T. Lepri and T. H. Zurbuchen, Space Physics Research Laboratory, University of Michigan, Ann Arbor, MI 48109-2143, USA. (slepri@engin. umich.edu; thomasz@umich.edu)